

NASA-TM-84287

NASA Technical Memorandum 84287

NASA-TM-84287 19830010622

The Stress-Corrosion Behavior of Al-Li-Cu Alloys: A Comparison of Test Methods

Patrick P. Pizzo, Ray P. Galvin, and Howard G. Nelson

September 1982

LIBRARY COPY

OCT 12 1982

LANGLEY RESEARCH CENTER
LIBRARY, NASA
HAMPTON, VIRGINIA

NASA

National Aeronautics and
Space Administration



mathematical model for the subject helicopter (UH-60A Black Hawk) was programmed for real-time operation. Flight data were obtained to validate the math model, and to develop models for the pilot control strategy while performing mission-type tasks. The validated math model is to be combined

ENTER:

45 2 2 RN/NASA-TM-84287

DISPLAY 45/2/1

83N21104** ISSUE 11 PAGE 1669 CATEGORY 26 RPT#: NASA-TM-84287

A-9057 NAS 1.15:84287 82/09/00 46 PAGES UNCLASSIFIED DOCUMENT

UTTL: The stress-corrosion behavior of Al-Li-Cu alloys: A comparison of test methods

AUTH: A/PIZZO, P. P.; B/GALVIN, R. P.; C/NELSON, H. G. PAA: A/(San Jose State Univ.)

CORP: National Aeronautics and Space Administration, Ames Research Center, Moffett Field, Calif. AVAIL.NTIS SAP: HC A03/MF A01

MAJS: /*COPPER/*CORROSION/*LITHIUM/*MICROSTRUCTURE/*POWDER METALLURGY

MINS: / ALLOYS/ CRACK PROPAGATION/ DEFORMATION/ ELECTROCHEMISTRY/ FRACTURE MECHANICS/ MORPHOLOGY/ STRAIN RATE

ABA: B. W.

ABS: The stress-corrosion (SC) behavior of two powder metallurgy processed (Al-Li-Cu) alloys with and without Mg addition in aqueous 3.5% NaCl solution has been investigated. Three test techniques were employed in the investigation: the alternate immersion testings of tuning fork specimens, slow crack-growth tests using fracture-mechanics specimens, and the slow strain-rate testing of straining electrode specimens. The corrosion conditions investigated include cathodic and anodic potentiostatic control and free-corrosion under constant-immersion and alternate-immersion conditions. The heat treatment and the orientation of the alloys were varied to establish the more susceptible material conditions. Scanning

ENTER:

DISPLAY 45/2/2

83N18893** ISSUE 9 PAGE 1335 CATEGORY 26 RPT#: NASA-TM-84287

A-9057 NAS 1.15:84287 82/09/00 46 PAGES UNCLASSIFIED DOCUMENT

UTTL: The stress-corrosion behavior of Al-Li-Cu alloys: A comparison of test methods

AUTH: A/RIZZO, P. P.; B/GALVIN, R. P.; C/NELSON, H. G. PAA: A/(San Jose State Univ.)

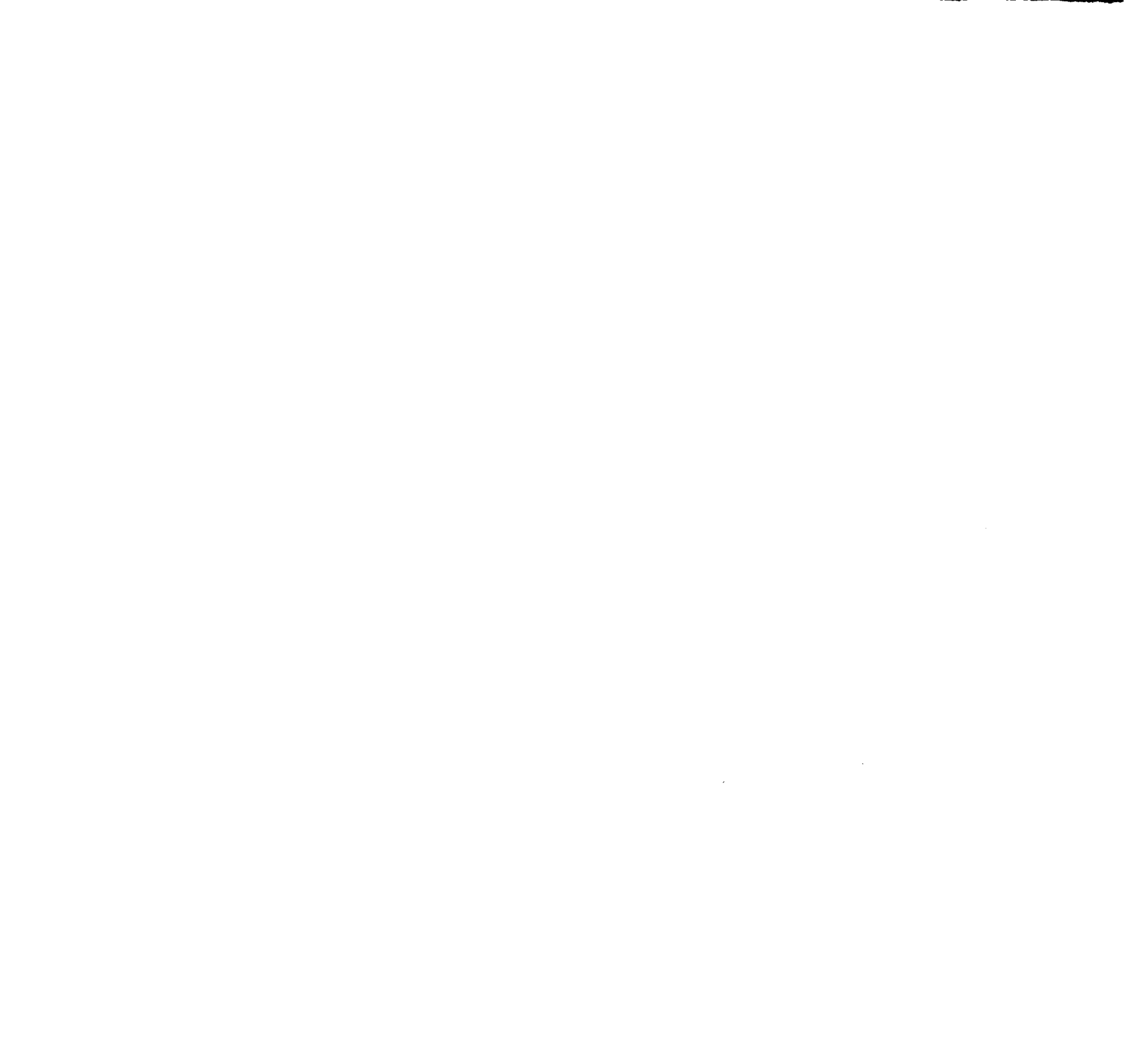
CORP: National Aeronautics and Space Administration, Ames Research Center, Moffett Field, Calif. AVAIL.NTIS SAP: HC A03/MF A01

MAJS: /*ALUMINUM ALLOYS/*COPPER ALLOYS/*CORROSION TESTS/*LITHIUM ALLOYS/*POWDER METALLURGY/*STRESS CORROSION

MINS: / AQUEOUS SOLUTIONS/ FRACTURE MECHANICS/ SALT BATHS/ SODIUM CHLORIDES/ STRAIN RATE/ STRESS CORROSION CRACKING/ TITRATION

ABA: A. R. H.

ABS: Two powder metallurgy processed (Al-Li-Cu) alloys with and without Mg addition were studied in aqueous 3.5% NaCl solution during the alternate immersion testing of tuning fork specimens, slow crack growth tests using fracture mechanics specimens, and the slow strain rate testing of straining electrode specimens. Scanning electron microscopy and x-ray



The Stress-Corrosion Behavior of Al-Li-Cu Alloys: A Comparison of Test Methods

Patrick P. Pizzo, San Jose State University, San Jose, California

Ray P. Galvin

Howard G. Nelson, Ames Research Center, Moffett Field, California



National Aeronautics and
Space Administration

Ames Research Center
Moffett Field, California 94035

1183-21104 #



Introduction

Aluminum-lithium alloys have received much recent attention because of the rather substantial specific-strength and specific-stiffness advantage offered over commercial 2000- and 7000-series aluminum alloys.⁽¹⁻³⁾ As an example, if one compares typical properties of the aluminum-lithium-copper (Al-Li-Cu) alloys of this investigation^(4,5) to AA 7075-T73 aluminum, the following approximate gains are realized: a 24 percent increase in the stiffness-to-weight ratio and a 14 and 18 percent increase in the strength-to-weight ratio based on yield strength and ultimate tensile strength, respectively. One obstacle in Al-Li alloy development has been the inherent limited ductility.⁽⁶⁻⁹⁾ Intense planar slip, due to the nature of the ordered, δ' (Al_3Li) precipitates responsible for strengthening, results in either slip-plane or grain-boundary decohesion,⁽¹⁰⁾ and thus deformation beyond the point of plastic instability is seldom observed.

Powder metallurgy (P/M) technology has been applied in current alloy development programs to provide a more homogeneous distribution of lithium and a more uniform, refined microstructure than that obtained by conventional ingot processing. Since the introduction in the mid-1950s of alloy X-2020, the first experimental ingot-processed lithium-bearing alloy (which saw limited aerospace application), the goal in Al-Li alloy development has been the improvement of tensile ductility and fracture toughness through processing, heat treatment, and compositional variations. The status of Al-Li alloy development is the subject of a pending review (Sanders, T. H., Jr. and Starke, E. A., Jr., International Metallurgical Reviews, in preparation).

Over the next decade, it is anticipated that advanced Al-Li alloys will see increased utilization in the design or major redesign of aerospace systems. Alloys will be selected on the basis of density, elastic modulus, and strength

to achieve major savings in weight, and thus reduce operational costs. To fully assess the specific-strength and specific-stiffness advantages of the candidate alloys, durability criteria, such as fatigue endurance and environmental-sensitive fracture, must be considered. Stress corrosion (SC) of high-strength aluminum alloys has been a major service problem in the aircraft industry. Thus, the specific-properties advantage of alternative alloys must be adjusted to account for their susceptibility to SC. At NASA Ames Research Center, current research is being directed toward an understanding of the environment-sensitive fracture mechanisms active in advanced Al-Li alloys. Attention has focused on Al-Li-Cu alloys because of the concurrent and extensive alloy development effort by others on this system^(8,10-13) and only limited corrosion and stress-corrosion data are available.^(14,15) A major objective of the current research program is to evaluate the relative SC resistance of two P/M processed Al-Li-Cu alloys.

Three different methods of determining the SC resistance of aluminum alloys were employed, and the results are reported herein. The aggressive environment for all tests is an aqueous NaCl solution. In the first test method, smooth-section specimens, under load, were exposed under alternate-immersion conditions to determine the threshold stress for SC. The threshold stress is defined as the upper limit stress below which specimens do not fracture during a specified exposure period. The second test method involved fracture-mechanics (flawed) specimens, tested to evaluate the threshold stress intensity factor for stress-corrosion cracking (SCC), K_{ISCC} . The threshold stress intensity factor is defined as that value at some limiting value of crack-growth rate. The third method involved slow strain-rate tests performed under potentiostatic polarization conditions to establish the active electrochemical regime for SC. In this paper, the apparent threshold stress, the

threshold stress intensity factor, and the slow strain-rate data are reported and compared. Metallographic and fractographic data are then introduced in an attempt to isolate SC behavior from other time-dependent processes active in the P/M processed Al-Li-Cu alloys.

Experimental

Materials

Al-Li-Cu Alloys

Two Al-Li-Cu alloys were purchased from Kawecki-Berylco Industries, Inc., Reading, Pennsylvania. The alloys were processed using P/M techniques. Powders were produced by cooling an atomized molten stream of the target composition in an inert gas (argon) atmosphere. High-purity (0.9999 percent by weight) aluminum and a 20 percent by weight lithium master alloy were combined to yield an approximate 2.6 percent Al-Li melt. High-purity-element additions were made to adjust the melt to the desired alloy composition. The cooling rate of the atomization process was estimated to be 10^3 Ks^{-1} . The resulting powders were spherical, about 150 μm in diameter (sized to 100 mesh).

Powders were packed in AA 6061 aluminum cans (13.7 cm outer diameter by 0.32 cm thick), degassed, and cold isostatic pressed to 415 MPa. The compacted powders were then hot-upset at 755 K against a blind die and extruded at 672 K through a 55.9-mm by 14.7-mm die. This yields an approximate 10:1 extrusion ratio. The chemical composition of the resulting alloys are presented in Table 1. The nominal composition of the base alloy is Al-2.6%Li-1.4%Cu and that of the magnesium-bearing alloy is Al-2.6%Li-1.4%Cu-1.6%Mg.

The microstructure, aging response, and mechanical properties of the two Al-Li-Cu alloys have been thoroughly documented in earlier reports. ^(4,5)

In Table 2, the tensile and fracture properties of the base alloy and the magnesium-bearing alloy are summarized for the three aging conditions investigated in this SC study: the under-, peak-, and over-aged conditions. Tensile properties of the base alloy at peak aging are 460 MPa yield and 550 MPa ultimate tensile strength, with a strain to fracture of 3 percent. In the magnesium-bearing alloy, yield and ultimate tensile strengths are 520 MPa and 600 MPa, and the strain to fracture is about 3.5 percent. Both alloys are characterized by limited deformation beyond plastic instability. Very little reduction in area is observed and fracture characteristics are brittle. The limiting fracture toughness for long transverse (1 in. wide by 1/2 in. thick) compact tension specimens (CTS) for both alloys was found to be about $8 \text{ MPa}\sqrt{\text{m}}$ and the fracture toughness was found to be relatively insensitive to the aging condition.⁽⁵⁾

High-Strength 700-Series Aluminum Alloys

In order to provide a basis for comparison of the SC behavior of the Al-Li-Cu alloys and to document the performance of a commercial alloy, concurrent alternate-immersion tests were conducted on specimens fabricated from AA 7075-T6 and AA 7475-T6 aluminum. The AA 7075-T6 aluminum specimens were fabricated from a square section 9 cm by 9 cm, forging; the AA 7475-T6 aluminum specimens were fabricated from commercial AA 7475-T7351 plate, 11.5-cm thick, and reheat-treated to the T6 condition prior to specimen fabrication. The chemical compositions of the 7000-series alloys are also reported in Table 1.

Test Methods

Method 1: Alternate-Immersion Tests

The tuning fork specimen⁽¹⁶⁾ selected for the alternate-immersion test program is illustrated in Fig. 1. A surface area of about 5 cm^2 is maintained

at constant stress using this specimen configuration. Aluminum-lithium-copper alloy tuning fork specimens were oriented to promote crack initiation along a plane whose normal is in the transverse (T) direction, and crack extension in the short transverse (S) direction. After fabrication, specimens were solution treated, quenched, and aged to the desired condition.

Tuning fork specimens were directly machined from the AA 7075-T6 aluminum and AA 7475-T6 aluminum alloy stock. The AA 7075-T6 aluminum specimens were oriented so that the crack plane and crack extension direction were both normal to the extrusion direction of the square-section stock. This orientation was selected because of the similar grain-abstract ratio to the Al-Li-Cu P/M extruded plate. The grain-abstract ratio is an important parameter in determining a material's SC performance.⁽¹⁷⁾ The AA 7475-T6 aluminum tuning fork specimens, fabricated from plate stock, were short-transverse oriented, thus presenting the least favorable microstructure from the standpoint of SC. This limiting microstructural condition could not be evaluated on the Al-Li-Cu alloys due to the thickness (1.27 cm) of the available Al-Li-Cu product form. After machining, the gage surfaces of the tuning fork specimens were rough polished to a 15 μm finish.

Both constant-deflection and constant-load tests were performed on the tuning fork specimens. Constant-deflection conditions were attained by single-bolt loading using two half-cylinder stainless steel platens, as shown in Fig. 1. The gage surfaces of these specimens were strain gaged to determine the initially applied, outer fiber stress and to signal specimen failure. Constant load conditions were attained using the platens and a dead-weight cable loading system. Initial, outer fiber stress was calculated using the elastic equation for a cantilever beam. Specimen failure was signaled using a linear voltage differential transformer (LVDT) attached to the load train.

The load assemblies were masked using a silicone lacquer and a paraffin wax topcoat. Both constant-deflection and constant-load specimens were exposed in an SC facility designed for alternate-immersion testing in a 3.5 percent NaCl solution as defined by ASTM Standard G44-75. Specimen failure was indicated by either change in the LVDT output from the load line of the constant load test, or from an abrupt decline in the strain-gage output from the instrumented constant-deflection specimens. A 32 channel analog-to-digital data acquisition system was used to periodically monitor and record test conditions.

Method 2: Slow Crack-Growth Tests

Double cantilever beam (DCB) specimens,⁽¹⁷⁾ as specified in Fig. 2, were used to assess K_{ISCC} . Specimens were fabricated from solution-treated and quenched Al-Li-Cu plates 3-1 oriented; that is, crack extension occurred on a plane normal to the short transverse direction and in the longitudinal (extrusion) direction. All specimens were aged and their sides polished to 1 μm using diamond paste. To monitor crack extension, reference lines were diamond scribed on the specimens.

Prior to aqueous NaCl exposure, the DCB specimens were fatigue precracked under strain control using a closed-loop servohydraulic test system. Precracking was performed at 10 Hz and the maximum stress intensity factor (K_{max}) during precracking did not exceed 80 percent of the initially applied K_I^i value for the SCC test. Precracking was performed in air, and the final crack length was approximately 18 mm.

The precracked DCB specimens were loaded using stainless steel bolts and the bolt-loaded end of each test assembly was masked using silicone lacquer and paraffin wax. Specimens were immersed in 3.5 percent NaCl solution 10 min prior to bolt loading and a clip-on extensometer was used to monitor crack-opening displacement. Specimens were loaded to initial stress-intensity

factors (K_I^I) ranging from 6 to 9 MPa \sqrt{m} . The upper limit of 9 MPa \sqrt{m} is approximately 85 percent of the average K_Q value determined in air for three peak-aged and S-L oriented, base alloy DCB specimens. After initial loading, the specimen was removed from the solution and crack length was determined by optical microscopy utilizing a calibrated traveling stage. Specimens were then reimmersed in the 3.5 percent NaCl solution and twice each week the specimens were removed and the crack extension determined using the optical technique. Unfortunately, localized crevice corrosion along the crack negated efforts to accurately determine crack length; therefore, this effort was abandoned after the 30-day immersion period. The solution was changed weekly in the approximate 1.0-litre immersion reservoir. Solution conditions were static, and the temperature of the solution was maintained at 30 deg C.

After an immersion period of about 35 days, the DCB specimens were unloaded and the crack-opening displacements were monitored using a clip-on extensometer to assess the degree of crack closure. Specimen sides were reconditioned on a metallographic polishing wheel with a deep nap polishing cloth; 3.5 percent NaCl solution was used as a lubricant. The current crack length was optically determined, and DCB specimens were reloaded to higher K_I^I values (greater crack-opening displacements). Specimens were reimmersed for an additional exposure period of 159 days.

Method 3: Slow Strain-Rate Tests

Straining Electrode Specimens- The straining electrode specimen shown in Fig. 3 was used for the slow strain-rate test. It is a standard tensile coupon fabricated from nominal 1.4-mm thick material machined from the extruded and solution-treated plate. Specimens were aged after fabrication and gage surfaces were rough polished to 400 grade emery paper prior to final specimen preparation.

The specimens were electrically isolated by applying end-tabs to the grip regions at the end of the specimen. The end-tabs consisted of a 0.25-mm thick aluminum shim cap bonded to the specimen using a room-temperature cured amine-epoxy system. Nylon net, 0.2-mm thick, was sandwiched between the specimen and the shim cap to assure electrical isolation. To complete electrical isolation during tensile testing, the load grips and loading pins were fabricated from Zircaloy-4 alloy plates. After fabrication, all zirconium pieces were pickled in a solution containing 120 ml H₂O, 40 ml HNO₃ (70 percent) and 3 ml HF (50 percent) and warm-water rinsed. This was followed by an oxidation treatment consisting of a 24-h hold at 530 deg C in an air furnace to develop a thick, electrically insulative ZrO₂ coating. The combination ZrO₂ and epoxy composite interface between the load-train and test specimen provided electrical isolation to the 4600-N load maximum required in this investigation.

The straining electrode specimens were strain gaged on opposing surfaces within the gage section (Fig. 3) to provide direct tensile strain measurements. After gaging, all specimen surfaces were coated with a solvent-thinned room temperature vulcanizing silicone rubber except a 4.8 mm by 9 mm unmasked region on one surface within the gage region (Fig. 3) where potentiostatic control was maintained. This unmasked region was final polished to a 1 μm diamond, acetone cleaned, and freon rinsed prior to coating the specimen.

Potentiostatic polarization methods were used in the slow strain-rate tests to establish and control electrochemical conditions. In preparation for the slow strain-rate tests, anodic potentiodynamic polarization data were obtained to establish the base electrochemical behavior of the Al-Li-Cu alloys. Cylindrical specimens with an electrode surface area of about 1.4 cm² were machined from extruded plates previously heat treated and cold-water quenched. These specimens were aged, polished on a bench lathe to a 1 μm diamond finish,

degreased in acetone, and then rinsed in freon. After being attached to the working electrode of the polarization cell, specimens were immersed in a stirred and helium-deaerated, 3.5 percent NaCl solution. After a maximum of 40 min, the potential was driven from a value more anodic than the rest-potential to a value more cathodic than the breakaway-potential and the current density versus potential response was monitored. A Wenking Model LT73 potentiostat and motor-driven scan generator were used to vary the electrochemical potential. The solution was deaerated by bubbling helium for 24 h prior to and during each scan. The potential scan rate of 10 mV/min and the current density versus potential curve was recorded on an X-Y recorder. Potentiodynamic measurements were made as described in ASTM G5-78, except for two minor variations found necessary to assure reproducibility of results. First, an extended deaeration and presoak period of up to 6 h was employed prior to initiation of the potentiodynamic scan. Second, because of safety considerations, helium was used to deaerate the polarization-cell solution as a substitute for the hydrogen recommended in ASTM G5-78. Effective deaeration of the polarization-cell solution proved the most critical step for reproducible potentiodynamic and potentiostatic measurements. Using the above method, anodic potentiodynamic polarization plots were obtained for the Al-Li-Cu alloys as a function of heat treatment. From these plots, electrochemical potentials were selected for the slow strain-rate tests.

To perform a slow strain-rate test, tensile specimens were first gripped and electrical isolation was confirmed. Next, a split, plastic base was affixed to the long end of the tensile coupon, adjacent the lower grip. A half-litre clear plastic cylindrical chamber was slipped over the upper grip and a rubber o-ring arrangement provided a water-tight seal at the base plate. A cylindrical rubber bellows provided helium cover gas containment while

allowing tensile displacement of the upper load grip. Helium-deaerated aqueous 3.5 percent NaCl solution was circulated through the test chamber from a 40-litre reservoir, at a flow rate of about 30 cc/min. The test chamber contained the required counter electrodes and Luggin probe as recommended in ASTM-G5 to establish potentiostatic conditions at the unmasked specimen surface. Thus, an essentially equivalent procedure to that described to obtain the potentiodynamic polarization data was used.

In addition to performing slow strain-rate tests under potentiostatic control in deaerated solution, one test was performed under open-circuit conditions at the free-corrosion potential of the alloy. For this test, the aqueous NaCl solution was brought to an equilibrium oxygen (O₂) solubility content by bubbling high-purity O₂ gas for 6 h before and during the test. Reference slow strain-rate tests were performed in laboratory air for comparison to the aqueous NaCl environmental tests.

Slow strain-rate tests were performed using a closed-loop servohydraulic test system interfaced with a PDP 11/34 computer. Strain, load, and displacement data were acquisitioned and the feedback conditions were computer adjusted to provide a constant engineering strain rate at the specimen gage during the test. Rates investigated ranged from 10^{-4} to 10^{-6} s⁻¹. At the start of each test, the specimens were initially ramped to a strain of 0.2 percent in 10 s, and then the strain rate was reduced to the required value. When potentiostatic control was employed, the electrochemical conditions were established for 20 min prior to load application. At specimen fracture, the potentiostat was disengaged, and the resulting stress versus strain curve was displayed.

Analysis

Scanning electron microscopy (SEM) and optical metallography were used to demonstrate the character of the interaction between the Al-Li-Cu alloys and

the environment for the various electrochemical conditions of this investigation. Corrosion products were chemically removed prior to SEM examination in the following manner. Specimens were rinsed in distilled water, and mechanically cleaned with a soft fiber bristle brush. Specimens were then immersed for 5 min in a solution of 15 g Alconox powder in 350 cc distilled water at 40 to 55 deg C followed by 5 min of ultrasonic cleaning in the same solution. Specimens were then rinsed thoroughly in distilled water. The sequence of deoxidizing solutions recommended in ASTM G1-72 for aluminum alloys was used to remove the remaining visible film. After cleaning, the specimens were gold sputter-coated to enhance image contrast in the SEM. Scanning electron microscopy examination at various stages of the cleaning procedure confirmed that the fracture and surface morphology of the Al-Li-Cu specimens were not significantly altered.

In order to investigate the possible correlation of surface pitting observed in the SC experiments to microstructural features, a tuning fork specimen was specially prepared and a sequential metallographic examination of the surface of the specimen corroded under controlled electrochemical conditions was performed. The gage section of the tuning fork specimen was polished to 0.3 μm alumina using conventional metallographic techniques. The specimen was then bolt loaded to a sustained outer-fiber stress of 415 MPa and mounted in a polarization cell, meeting the requirements of ASTM G5-78. The entire tuning fork specimen was masked with silicone lacquer except for a 1.0-cm² area in the gage region of one arm. The specimen was positioned in the polarization cell and polarized in deaerated 3.5 percent NaCl solution at an applied potential of $-0.820 \text{ V}_{\text{sce}}$. A 16-h exposure period was interrupted at half-hour intervals to metallographically evaluate the surface condition. The surface was distilled water rinsed and air dried prior to metallographic examination.

Results

Alternate-Immersion Tests

Alternate-immersion tests were conducted on tuning fork specimens under free-corrosion conditions. Time to failure as a function of the applied stress is shown in Fig. 4 for the two Al-Li-Cu alloys and the AA 7075-T6 aluminum alloy. The AA 7075-T6 aluminum alloy was loaded to three stress levels between 415 and 440 MPa but did not fail nor show any evidence of cracking; however, pitting on these specimens was extensive. Conversely, both Al-Li-Cu alloys failed at 415 MPa after only a few hundred hours of exposure. The magnesium-bearing alloy failed at 378 MPa after less than 10^3 h exposure to alternate immersion. Cracking was also observed in both of the Al-Li-Cu alloys at runout (2×10^3 h) indicating that the threshold for SC is below 380 MPa for the base alloy and 350 MPa for the magnesium-bearing alloy. Obviously, both Al-Li-Cu alloys are more susceptible to SC than the AA 7075-T6 aluminum alloy under the conditions of our study, with the magnesium-bearing alloy being the most susceptible.

Typical SC crack morphology observed on the surface of the tuning fork specimens of both Al-Li-Cu alloys is shown in Fig. 5. As can be seen, after about 2×10^3 h of exposure to alternate immersion, the surface of these specimens are only mildly pitted but do contain numerous stress-corrosion cracks as deep as 0.3 mm, as shown in Fig. 6. These cracks appeared to be generally intergranular and severely branched, as is evident in Fig. 6(b).

Slow Crack-Growth Tests

Slow crack growth in the Al-Li-Cu alloys was studied using bolt-loaded, DCB-type, fracture-mechanics specimens continuously exposed to an aqueous 3.5 percent NaCl environment under free-corrosion conditions. Because of the problem of extensive crevice corrosion along the edge of the crack, optical

measurements of the crack length could not be used. Instead, crack extension was determined after specimen failure from an analysis of the fracture surface. The specimens were removed from the solution after 8.4×10^2 h of exposure, unloaded to estimate any change in specimen compliance, reloaded to a higher applied stress, and exposed to the test environment for an additional 3.8×10^3 h. Considerable crack closure was observed during the unloading of all exposed specimens, after both short-term and long-term exposure.

Table 3 is a summary of these data for the base alloy in the under-aged and peak-aged conditions and for the magnesium-bearing alloy in the over-aged condition. Tests are continuing on both alloys in these and other heat-treatment conditions, and will be terminated after approximately 1×10^4 h of exposure and reported elsewhere. Shown in Table 3 are the initially applied stress intensity, K_I^i ; the final stress intensity, K_I^f ; and the estimated crack extension for the two exposure intervals. All specimens gave some indication of crack extension as the result of the exposures with the exception of the peak-aged, base alloy specimen exposed for the shortest time. This specimen exhibited crack pop-in during initial loading (the initially applied K exceeded K_Q of the material and did not exhibit detectable crack growth).

After the last immersion test, all specimens were pulled to failure and their fracture surfaces were analyzed. Figure 7 is an overview of the failure surface of the magnesium-bearing alloy and is typical. In all cases the regions of fatigue crack growth, crack extension during short-term exposure, crack extension during long-term exposure, and rapid unstable crack extension could easily be distinguished macroscopically, prior to cleaning, and were used to calculate crack extensions (Table 3). This was not the case, however, microscopically and following cleaning. A detailed SEM analysis of all failed specimens was unable to identify any significant variation in fracture topography

associated with short- and long-term immersion and rapid, unstable fracture. As an example, areas of crack growth associated with long-term immersion and unstable fracture are shown in Fig. 8 for the magnesium-bearing alloy. Although the details of the fracture are somewhat masked as the result of corrosion and the required cleaning procedures, the magnesium-bearing alloy appears to have failed in a duplex mode with coarse intergranular regions bounded by fine intergranular regions. These regions can be correlated with variations in the microstructure.⁽⁴⁾ The overall fracture topography of the base alloy differs somewhat from the magnesium-bearing alloy but is simply a reflection of differences in microstructure. Differences in the various regions of crack growth remain indistinguishable.

Slow Strain-Rate Tests

Slow strain-rate tests were conducted using the straining electrode specimens of the Al-Li-Cu base alloy under a variety of electrochemical conditions. The standard potentiodynamic polarization data had been obtained previously.⁽⁵⁾ One such curve for the base alloy composition is shown in Fig. 9 and is generally typical of both Al-Li-Cu alloys over the range of aging treatments investigated. In this figure, the passive regime occurs along the voltage-independent, current density plateau. In this regime, a passive corrosion film is formed. The aging condition has little systematic influence on the passive current density. However, a slight decrease (more negative potential) in breakaway potential occurred for the longer aging times. On occasion, current spikes were observed along the plateau, indicating instability of the passive film. Nevertheless, the potentiodynamic technique proved relatively insensitive to microstructural variations which occur for the under-, peak-, and over-aged conditions.

Slow strain-rate tests were performed at three electrochemical conditions based on the data similar to Fig. 9: (1) anodic potentiostatic control at $-0.850 V_{sce}$ in a deaerated solution, (2) cathodic potentiostatic control at $-1.075 V_{sce}$ in a deaerated solution, and (3) open-circuit potential under free-corrosion conditions in an oxygenated solution. Additionally, tests were performed in a laboratory-air environment for comparison. The SC susceptibility of Al-Li-Cu alloys at various electrochemical conditions is indicated in Fig. 10. Plotted in this figure are strain-to-fracture (ϵ_f) data as a function of the applied strain rate. The control tests performed in air and the specimen tested under cathodic potentiostatic control exhibited a strain to fracture (ϵ_f) of about 6.5 percent. In air, ϵ_f was found to be strain-rate independent over the range of strain rates investigated. However, anodic potentiostatic control resulted in a linear decline in ϵ_f from 4.6 percent at $10^{-4} s^{-1}$ to less than 2.0 percent at $10^{-6} s^{-1}$. Free corrosion in an oxygenated NaCl solution at $10^{-6} s^{-1}$ resulted in an ϵ_f of 4.5 percent — a modest decrement of about 2 percent in strain with respect to that observed in air.

The mode and topography of fracture and the condition of the unmasked surface was studied on each of the failed specimens (Fig. 10). Failure in air occurred at random along the gage length of the specimens. In general, cracking occurred in shear by a single crack oriented 45 deg to the loading direction (the common mode of failure in all base alloy specimens). The fracture path was transgranular and occurred by microvoid coalescence. The specimen exposed to cathodic potentiostatic control exhibited a similar value of ϵ_f as observed in air (Fig. 10); failure occurred across the masked region of the gage section, and failure was again transgranular by microvoid coalescence. The unmasked surface of the cathodic specimen exhibited uniform rows of small pits along the

direction of the load axis which is also the extrusion direction of the alloy and is shown in Fig. 11. As will be indicated, similar rows of pits were observed on the unmasked surfaces of all specimens exposed to the aqueous 3.5 percent NaCl solution. Also observed on the unmasked surface of the cathodic specimen (Fig. 11) are larger pits which are randomly arranged. Because failure occurred away from the unmasked region, neither type of pit contributed to the fracture process.

All specimens exposed to anodic potentiostatic control (Fig. 10) failed through the unmasked portion of their gage sections. Failures again occurred by shear with the general fracture path being transgranular with extensive microvoid coalescence. The unmasked surfaces contained rows of small pits and randomly arranged larger pits, similar to that observed in the cathodic specimen (Fig. 11), with the larger pits being the most severe at the lowest strain rate. Also, at the lowest strain rate the primary fracture did not occur on a single plane but was jagged at ± 45 deg to the load axis. Secondary shear cracks were observed in the vicinity of the primary fracture, as shown in Fig. 12. These secondary cracks seem to be associated with the larger pits; a number of larger pits were found along the edge of the primary crack, as shown in Fig. 13. The intergranular nature of these pits is clearly evident in Fig. 13(b).

The specimen tested under free-corrosion conditions in an oxygenated solution (Fig. 10) failed by shear across the unmasked region of the specimen along a single fracture plane 45 deg to the loading axis. No secondary cracks were observed on the specimen surface and the primary crack appeared to initiate from a single, large pit near the surface of the specimen, as shown in Fig. 14(a). Figure 14(b) is the interior surface of this large pit. This surface is severely dimpled from the corrosion reaction and exhibits little or

no evidence of intergranular attack. The unmasked surface of this specimen contained the usual rows of small pits, but in addition a fairly uniform distribution of large patches of severe pitting was observed, as shown in Fig. 15. It was the large pit below one such patch that initiated the primary fracture (Fig. 14(a)).

In an attempt to correlate pitting with specific microstructural features, the surface of a specimen was metallographically polished and etched and subsequently stressed to 415 MPa and exposed to a static solution for 16 h under anodic potentiostatic control. Figure 16(a) shows the underlying microstructure of the alloy and the corresponding surface pits following exposure. Alloy microstructure consists of columnar bands of recrystallized grains bounded by strings of secondary particles aligned parallel to the extrusion direction. Although not shown, a few large particles (20 to 100 μm in diameter) were observed to be distributed randomly throughout the microstructure. These are thought to be master alloy inclusions carried over from the melt during the atomization P/M process.⁽⁴⁾ Surface pitting following exposure (Fig. 16(b)) appears to be associated with the selective attack of the secondary particles which are aligned parallel to the extrusion direction. The larger pits also appear associated with these particles and begin to develop after about 4 h of exposure. The large master alloy inclusions seem to play no role in the pitting process.

Discussion

Both Al-Li-Cu alloys, with and without a magnesium addition, appear to be susceptible to SC in an aqueous 3.5 percent NaCl solution under the right electrochemical conditions. Small surface pits are initially formed under all corrosion conditions investigated (cathodic and anodic potentiostatic control and under free-corrosion for both constant and alternate immersion) and are

associated with second-phase particles strung along the extrusion direction (Fig. 16). With time, larger pits are developed from these rows of smaller pits at selected locations across the exposed surface. Under cathodic control in a deaerated solution, the larger pits are randomly positioned, are shallow and flat bottomed, appear to be associated with a general corrosion attack (Fig. 11), and do not degrade the mechanical behavior (ϵ_f) of the alloy as determined by slow-strain rate tests (Fig. 10). Under anodic potentiostatic control in a deaerated solution, the larger pits are randomly positioned (Fig. 12) but appear to be formed by a selective dissolution mechanism associated with the grain boundaries of the alloy (Fig. 13(b)). At low strain rates (long exposures), numerous cracks are associated with these pits (Fig. 12) and significant mechanical degradation (ϵ_f) of the alloy is observed (Fig. 10). Under free-corrosion conditions in an oxygenated solution, a fairly uniform distribution of large patches of severe pitting is observed (Fig. 15). Although the corrosion process is somewhat selective, deep pits are formed (Fig. 14(a)) having dimpled interior surfaces (Fig. 14(b)) with no evidence of intergranular attack. Some degradation in mechanical behavior (ϵ_f) is observed (Fig. 10).

An estimate of the critical-flaw size required for unstable, rapid crack growth in the base Al-Li-Cu alloy under conditions of the slow strain-rate tests was made using a fracture-mechanics analysis. Assuming a surface flaw having an aspect ratio of about 0.5 (Figs. 13 and 14(a)), the critical flaw size is estimated to be approximately 0.25 to 0.30 mm. Based on this estimate, it is deduced that the reduction in mechanical behavior (ϵ_f) observed under free-corrosion conditions in an oxygenated solution (Fig. 10) is simply the result of the large corrosion pit [approximately 0.31 mm deep (Fig. 14 (a))] and does not involve significant stress-corrosion crack growth. Under anodic

potentiostatic control (Fig. 10), this is not the case. The moderate size of the intergranular surface pit (approximately 0.10 mm deep (Fig. 13)) suggests that slow crack growth did occur ahead of the pit — most probably as the result of the corrosive environment. However, no evidence of a change in fracture morphology was observed near these pits, as compared with the region of rapid, unstable crack growth. Unfortunately, much of the details on the fracture surface were masked as the result of corrosion following failure and the required surface-cleaning procedure.

Slow crack growth was observed under conditions of free corrosion in both Al-Li-Cu alloys at all aging conditions investigated (Table 3). Although the initially applied stresses on these precracked, fracture mechanics-type specimens were high, resulting in stress-intensity factors approaching the critical stress intensities, the extensive slow crack growth seems to support some contribution from the corrosive environment. Severe crevice corrosion was observed at the edges of the cracks (Fig. 7), as would be expected from the extensive pitting observed under similar electrochemical conditions in the slow strain-rate studies (Fig. 14(a)). However, within the specimen, along the crack tip, this extensive corrosive attack was not observed. Obviously, the actual electrochemical state along the crack front differs from that at the external surface but cannot be defined. The fracture morphology in the regions of slow crack growth and rapid, unstable fracture (Fig. 7) do not appear significantly different. Again, this may be the result of corrosion following the formation of the crack surfaces and the required surface-cleaning procedure.

Tests performed on the Al-Li-Cu alloys under alternate-immersion conditions had the longest exposure to a corrosive environment and were the most severely attacked. Additionally, in these tests the orientation of the material was such that the second-phase particles strung along the extrusion

direction lie perpendicular to the major axis of loading. Rows of small pits were formed at these particles but were less numerous than in the slow strain-rate tests and only a few larger pits were developed. Where rows of small pits did occur, cracks were initiated along the rows (perpendicular to the loading direction) and grew with time (Fig. 5). The general nature of these cracks appears to be similar to the pits observed in the slow strain-rate tests under anodic control (Fig. 13), that is, intergranular and severely branched (Fig. 6), but closed and significantly deeper. A fracture mechanics analysis of secondary surface cracks and cracks on unfailed specimens (Fig. 4) revealed that crack depth is approaching the critical flaw size for rapid, unstable crack growth in these specimens. Thus, unlike the anodic-controlled, slow strain-rate specimens, slow crack growth in these alternate-immersion specimens appears to occur by a singular mechanism involving the selective attack along the grain boundaries perpendicular to the major axis of loading.

Summary

The SC behavior of two Al-Li-Cu alloys, with and without a magnesium addition, was studied using three test methods: (1) threshold stress tests on tuning fork specimens, (2) slow crack-growth tests on fracture mechanics-type specimens, and (3) slow strain-rate tests on straining electrode specimens. Additionally, other experimental parameters were varied including constant versus alternate immersion in the aqueous 3.5 percent NaCl environment, deaerated versus oxygenated solutions, electrochemical potential (anodic, cathodic, and free-corrosion), and the orientation of the alloys. Each of these test methods was found to yield important information on the SC behavior of the Al-Li-Cu alloys.

Under all conditions investigated, second-phase particles strung out in rows along the extrusion direction in the alloys were the most rapidly attacked

and play a significant role in the SC process. With time, larger pits develop from these rows of smaller pits. Under cathodic potentiostatic control in a deaerated solution, these surface pits were shallow and flat bottomed and played no role in the fracture process. Under anodic control in a deaerated solution the large surface pits were shallow but intergranular. Surface cracks initiated from these pits and contributed significantly to the fracture process. Pit depth was considerably less than the critical flaw size for rapid, unstable crack growth in these materials, suggesting that chemically enhanced slow crack growth occurred by some other mechanism, such as hydrogen. Under free-corrosion conditions in an oxygenated solution, when the second-phase particles are aligned with the loading axis, massive, relatively open pits are formed which approach the critical flaw size in these materials and contribute directly to failure.

Slow crack growth was observed in the limited aging conditions investigated in both the Al-Li-Cu base alloy and the alloy containing magnesium. Although free-corrosion conditions were maintained, the fracture surfaces away from the specimen surface showed no evidence of gross chemical attack, again suggesting the possible role of hydrogen in the SC cracking process.

Finally, the indication of threshold stress for SC in both Al-Li-Cu alloys was found to be significantly lower than that observed for the 7075-T6 aluminum alloy and was the lowest for the magnesium-bearing alloy. In these tests, second-phase particles were oriented perpendicular to the loading direction, crack initiated along the rows of small surface pits, and grew with time. These cracks were closed and grew intergranularly with premature failure occurring as the cracks approached the critical flaw size in these materials.

Both Al-Li-Cu alloys, with and without a magnesium addition, are susceptible to SC in an aqueous 3.5 percent NaCl solution under the right conditions.

The susceptibility of these materials is very much influenced by both the electrochemical conditions present during the corrosion process and the microstructure of the alloys.

Acknowledgments

The authors acknowledge NASA support of this research effort through Contract NAS2-10365 and Cooperative Agreement NCC2-155 with San Jose State University. In addition, NASA is acknowledged for providing coauthor, Ray Galvin, with materials research experience through a cooperative work study program with DeAnza College of Cupertino, California.

References

- [1] Sanders, T. H., Jr. and Balmuth, E. W., Metallurgical Progress, Vol. 113, 1978, p. 32.
- [2] Balmuth, Edward S. and Schmidt, Richard, Aluminum-Lithium Alloys, T. H. Sanders, Jr. and E. A. Starke, Jr., Eds., AIME, 1981, p. 69.
- [3] Lewis, R. E., Webster, D., and Palmer, I. G., AFML Contract F33615-77-C-5186; Technical Report AFML-TR-78-102, July 1978.
- [4] Pizzo, P. P., NASA Report CR-166339, National Aeronautics and Space Administration, Washington, D.C., Ames Research Center Contract NAS2-10365, Sept. 1980.
- [5] Pizzo, P. P., NASA Report CR-3578, National Aeronautics and Space Administration, Washington, D.C., Ames Research Center Contract NAS2-10365, Jan. 1982.
- [6] Sanders, T. H., Jr., NADC Contract N62269-76-C-0271, Final Report, June 1979.
- [7] Gayle, F. W., Aluminum-Lithium Alloys, T. H. Sanders, Jr. and E. A. Starke, Jr., Eds., AIME, 1981, p. 119.
- [8] Webster, D., Metallurgical Transactions, Vol. 10A, Dec. 1979, p. 1913.
- [9] Gysler, A., Crooks, R., and Starke, E. A., Jr., Aluminum-Lithium Alloys, T. H. Sanders, Jr. and E. A. Starke, Jr., Eds., AIME, 1981, p. 263.
- [10] Lin, F. S., Chakraborty, S. B., and Starke, E. A., Jr., Metallurgical Transactions, Vol. 13A, March 1982, p. 401.
- [11] Lewis, R. E., DARPA Order 3417, Status Report (LMSC/D770654), June 1980.
- [12] Pao, P. S., Sankaran, K. K., and O'Neal, J. E., Aluminum-Lithium Alloys, T. H. Sanders, Jr. and E. A. Starke, Jr., Eds., AIME, 1981, p. 307.
- [13] Sankaran, K. K. and Grant, N. J., Aluminum-Lithium Alloys, T. H. Sanders, Jr. and E. A. Starke, Jr., Eds., AIME, 1981, p. 205.

- [14] Evancho, J. U., Naval Air Development Center Contract N62269-73-C-0219, Final Technical Report (Feb. 8, 1973-Feb. 7, 1974), June 1974.
- [15] Niskanen, P., Sanders, T. H., Jr., Rinker, J. G., and Marek, M., Corrosion Science, Vol. 22, No. 4, 1982, p. 283.
- [16] Craig, H. Lee, Jr., in Stress Corrosion Testing, ASTM STP 425, American Society for Testing Materials, 1967, p. 3.
- [17] Mostovoy, Sheldon, Crosley, P. P., and Ripling, E. J., Journal of Materials, Vol. 2, No. 3, Sept. 1967, p. 661.

Table 1 - Chemical composition of the aluminum alloys studied.

Alloy	Composition, wt %											ppm			
	Nominal alloy composition											O	Ca	Na	K
	Li	Cu	Mg	Zr	Si	Fe	Mn	Zn	Ti	Cr	Be				
Base, Al-Li-Cu	2.6	1.4	0.006	0.09	0.03	0.06	0.005	0.02	0.03	0.002	0.005	6	3	2	1
Mg-bearing, Al-Li-Cu-Mg	2.6	1.4	1.6	0.09	0.03	0.05	0.005	0.02	0.03	0.002	0.005	5	3	1	1
AA 7075 aluminum	-	1.49	2.27	0.01	0.07	0.21	0.03	5.51	0.04	0.21	-	-	-	-	-
AA 7475 aluminum	-	1.42	1.95	-	0.04	-	0.01	5.42	0.03	0.24	-	-	-	-	-

Table 2 — Typical mechanical properties of the Al-Li-Cu alloys as a function of aging condition.

Property ^a	Base alloy ^b			Mg-bearing alloy ^c		
	Aging condition ^d			Aging condition ^e		
	Under	Peak	Over	Under	Peak	Over
Yield stress (0.2% offset), MPa	385	460	420	455	520	435
Ultimate tensile stress, MPa	490	550	490	570	600	550
Strain to fracture, %	3.5	3.0	5.0	3.5	3.5	4.0
Fracture toughness K _Q , MPa√m	12	9	8.5	9.5	8.5	7.5

^aTensile data for 0.25-in. diameter standard tensile specimens; fracture toughness of 0.5-in. thick, 1-in. compact tension specimens.

^bBase alloy specimens solution treated at 788 K for 1 h plus cold-water quenching prior to aging.

^cMg-bearing specimens solution treated at 828 K for 1 h plus cold-water quenching prior to aging.

^dUnder-, peak-, and over-aged conditions are 10, 26, and 200 h at 443 K, respectively.

^eUnder-, peak-, and over-aged conditions are 5, 26, and 80 h at 463 K, respectively.

Table 3 - Time dependent crack growth of DCB specimens
in aqueous 3.5% NaCl solution^a

Alloy	Aged condition	35 day immersion			159 day immersion		
		K_I^i	K_I^f	$\Delta a,$	K_I^i	K_I^f	$\Delta a,$
		MPa \sqrt{m}		mm	MPa \sqrt{m}		mm
Al-Li-Cu	Under	9.0	7.5	3.0	9.5	7.5	2.5
Al-Li-Cu	Peak	11.0	9.0	0 ^b	9.0	8.5	0.8
Al-Li-Cu-Mg	Over	7.0	5.5	4.0	10.5	7.5	4.0

^a K_I^i : crack tip stress-intensity factor applied prior to immersion period. K_I^f : crack tip stress-intensity factor at termination of the immersion period.

^bExhibited pop-in during loading.

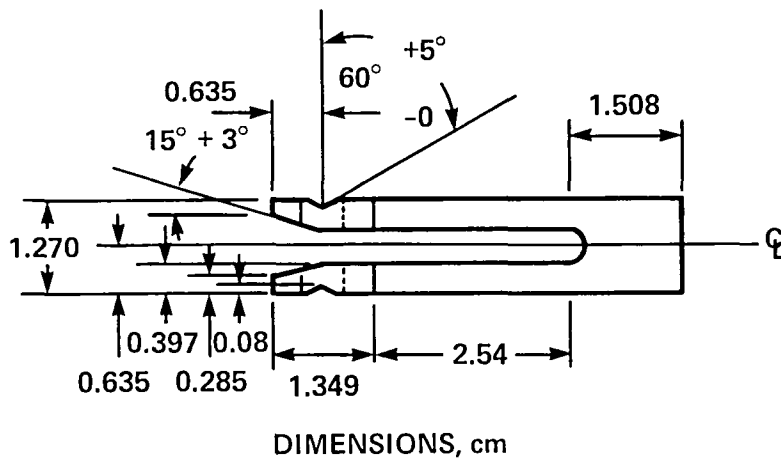
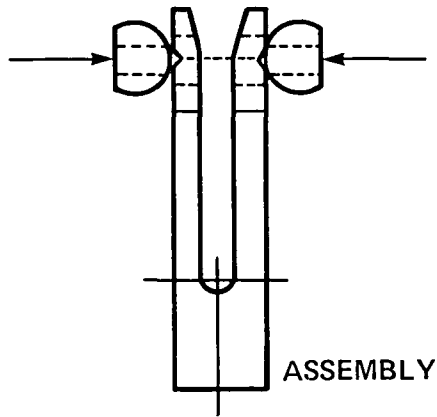
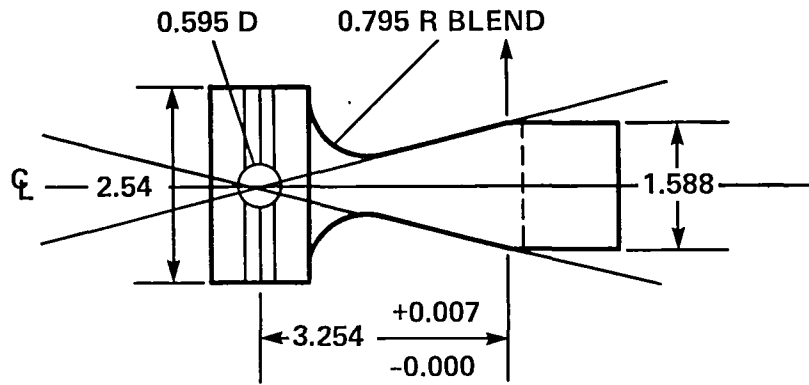


Figure 1.- Tuning fork specimen.

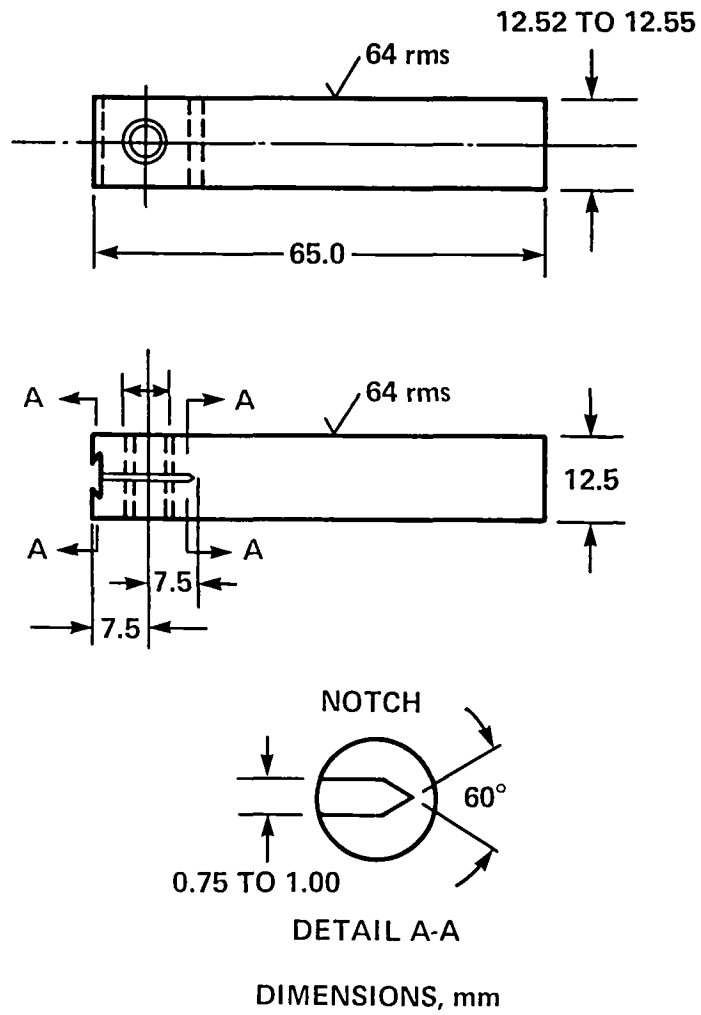
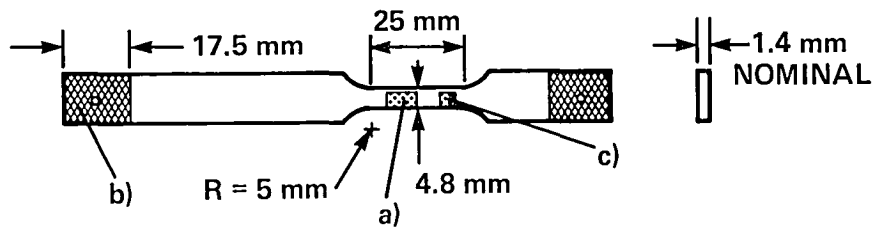


Figure 2.- Double cantilever beam (DCB) specimen.



- a) 9 mm BY 4.8 mm UNMASKED REGION ON ONE SIDE FOR POTENTIOSTATIC POLARIZATION.
- b) GRIP REGION FOR APPLICATION OF ELECTRICALLY INSULATIVE TABS.
- c) STRAIN GAGE LOCATION; TYPICAL, BOTH SIDES.

Figure 3.- The straining electrode specimen.

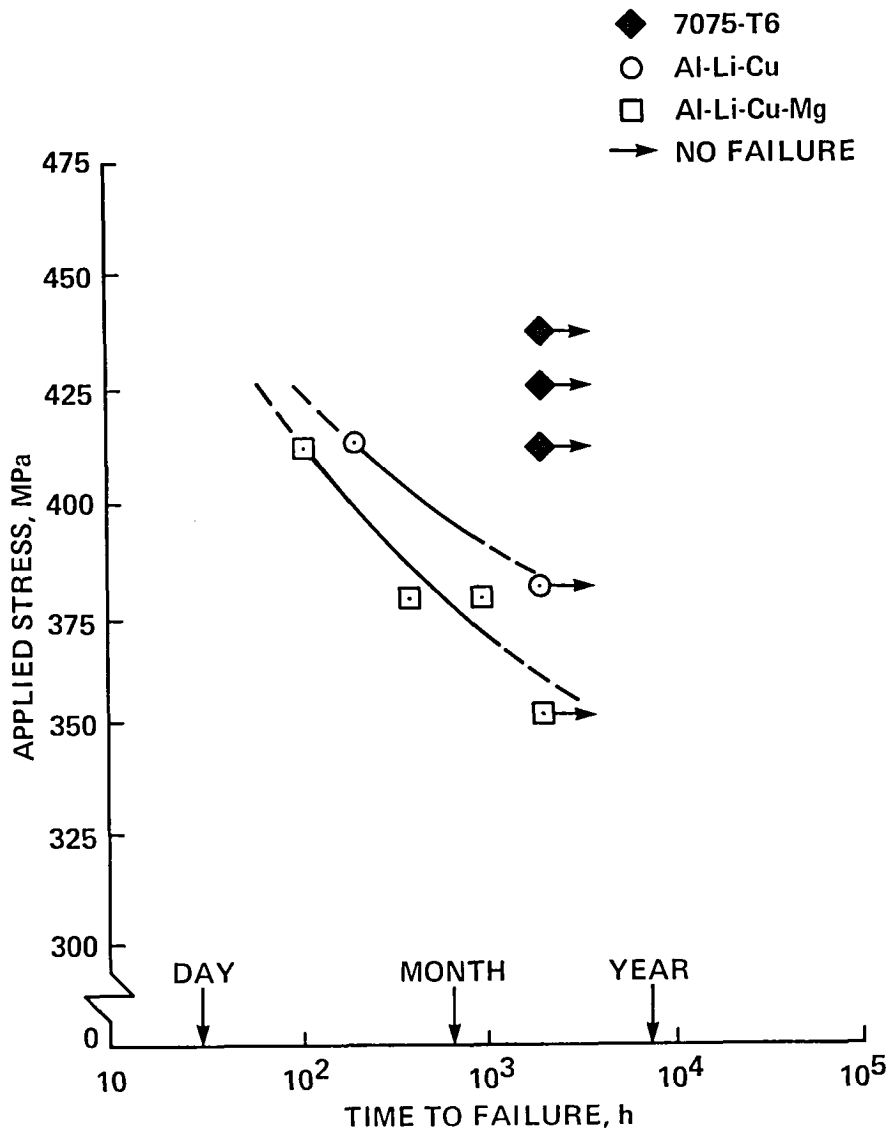


Figure 4.- The relative SC behavior in aqueous 3.5% NaCl solution under conditions of alternate immersion.

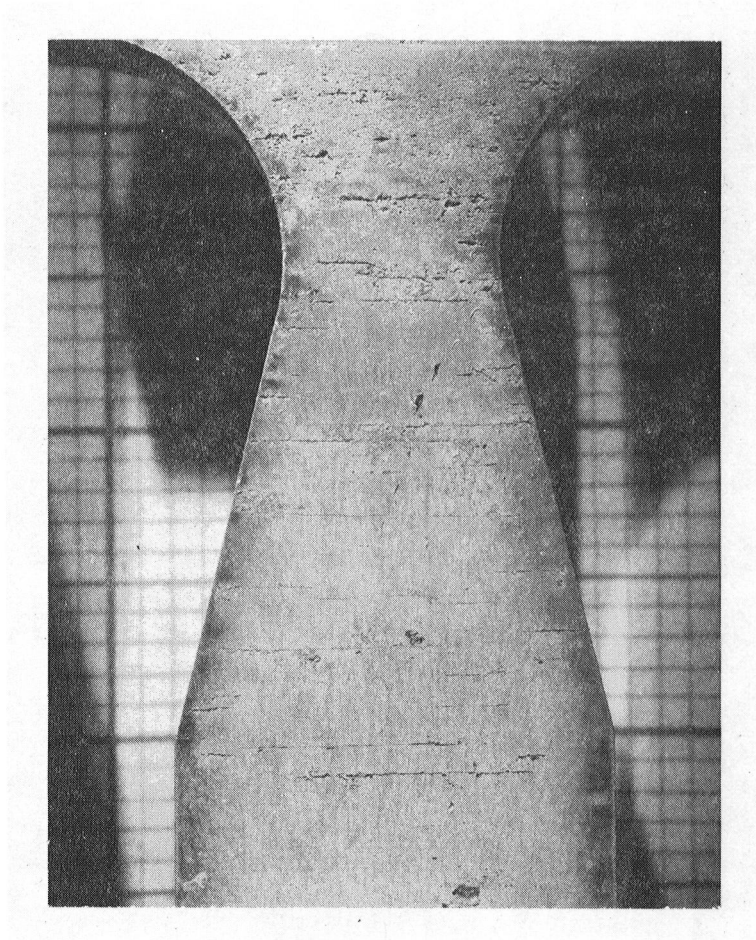


Figure 5.- Multicrack initiation on the tensile surface of an Al-Li-Cu alloy tuning fork specimen after an 84-day alternate immersion exposure in aqueous 3.5% NaCl solution.

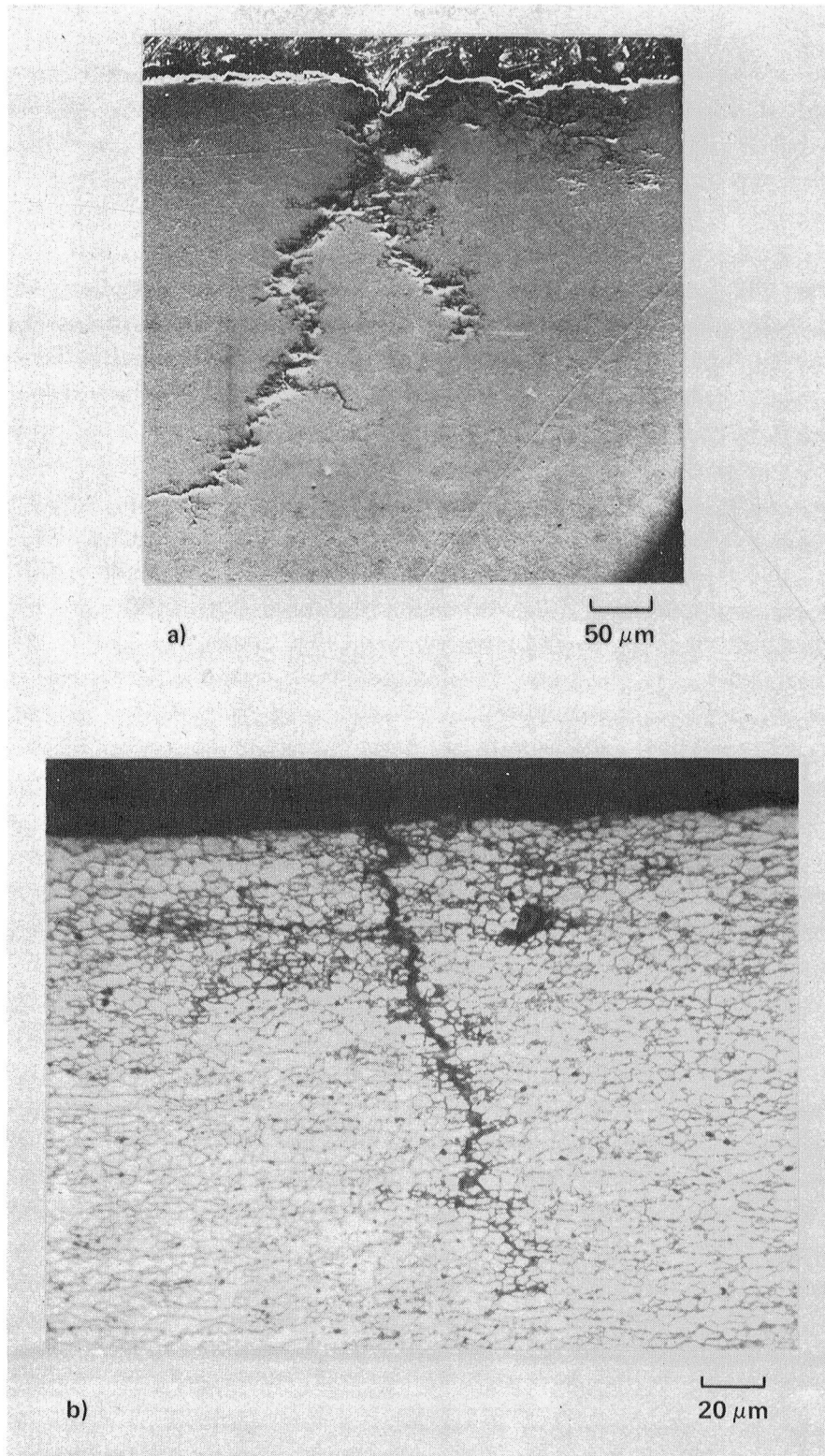


Figure 6.- Stress corrosion cracks in the Al-Li-Cu-Mg alloy, edge of tuning fork specimen: (a) SEM micrograph of a surface crack. (b) Optical micrograph of a second crack indicating the intergranular, multibranched fracture path.

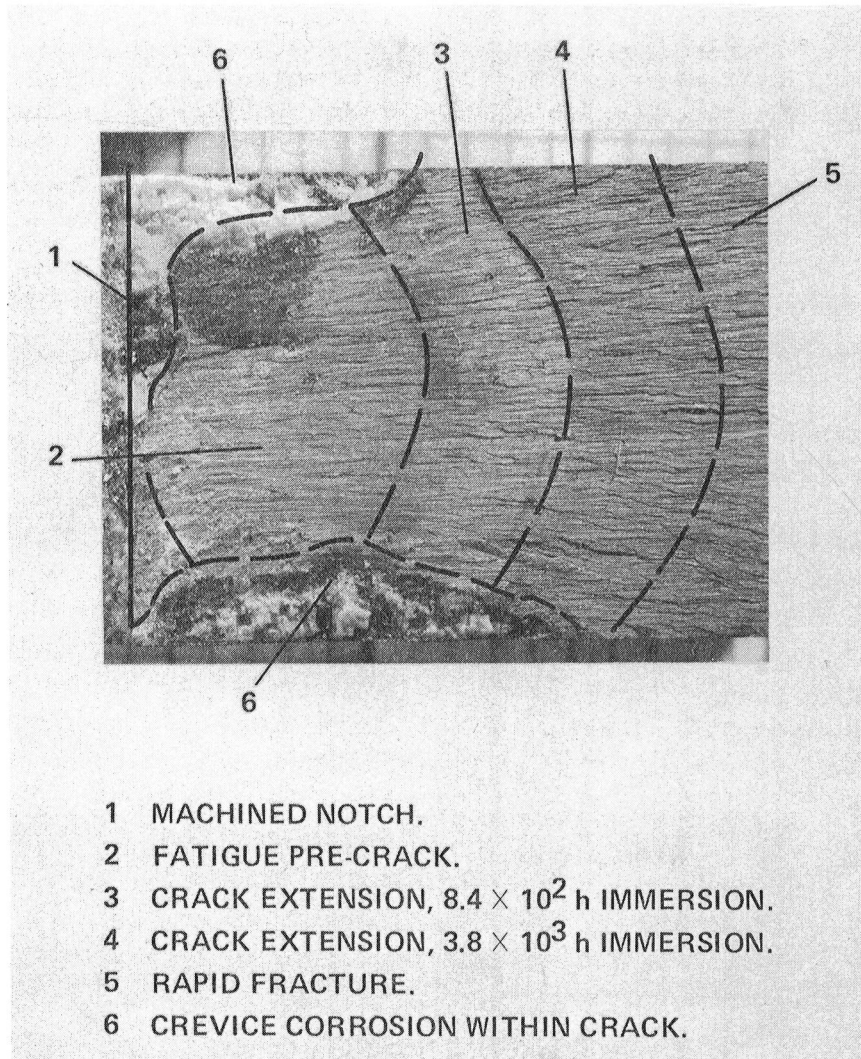


Figure 7.- Fracture surface of Al-Li-Cu-Mg alloy DCB specimen showing the various regions of crack growth,

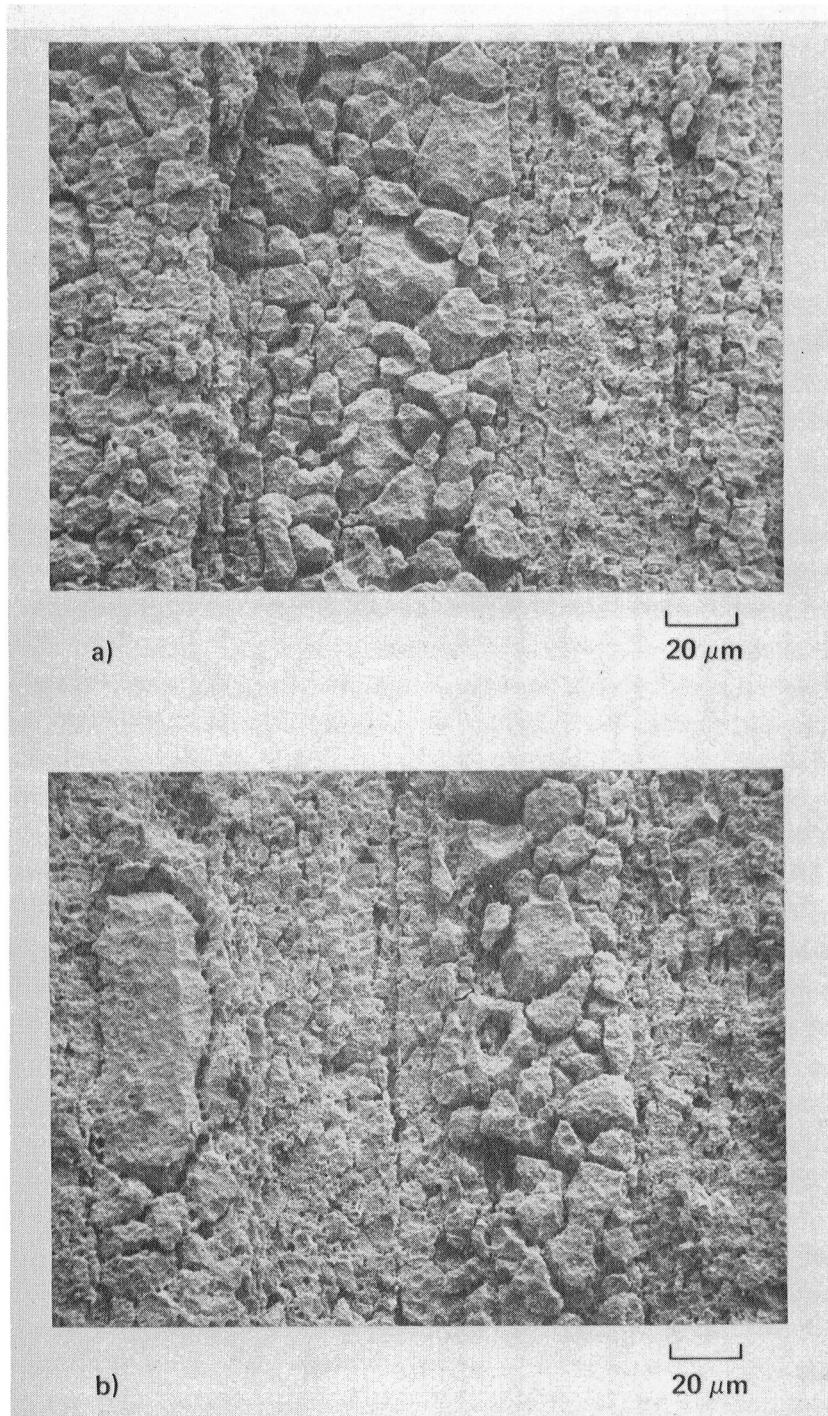


Figure 8.- The fracture topography of the DCB specimen of figure 7: (a) Time-dependent crack extension, Region 3. (b) Rapid fracture, Region 5,

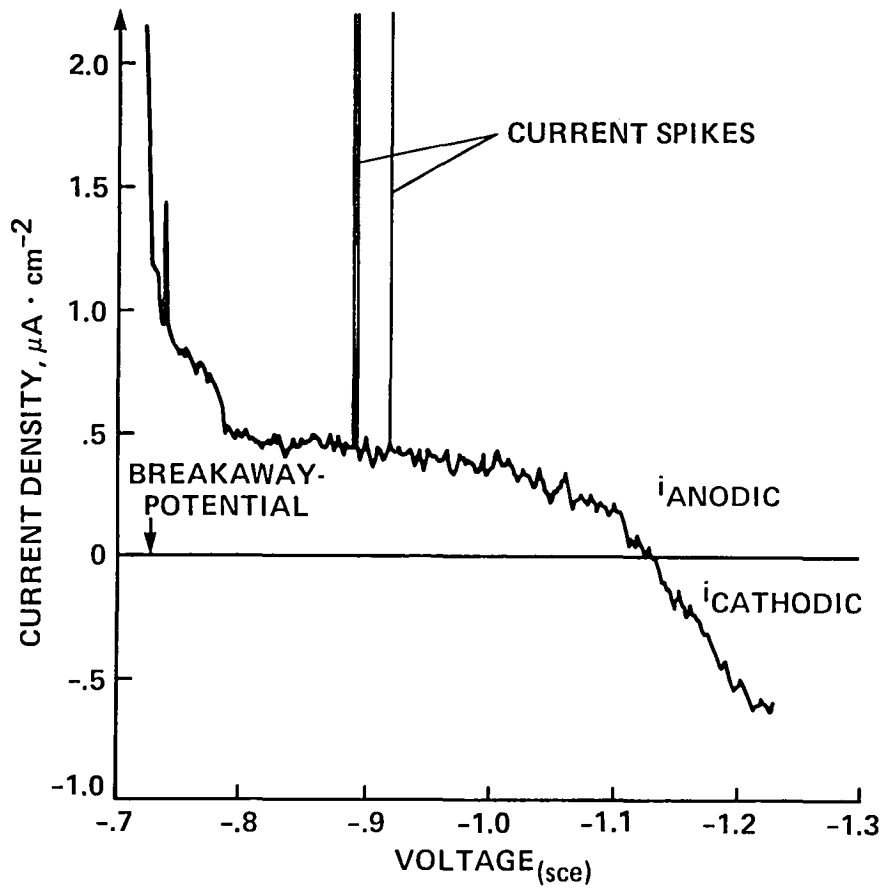


Figure 9.- Electrochemical characteristics of peak-aged Al-Li-Cu alloy determined by potentiodynamic scan in deaerated aqueous 3.5% NaCl solution,

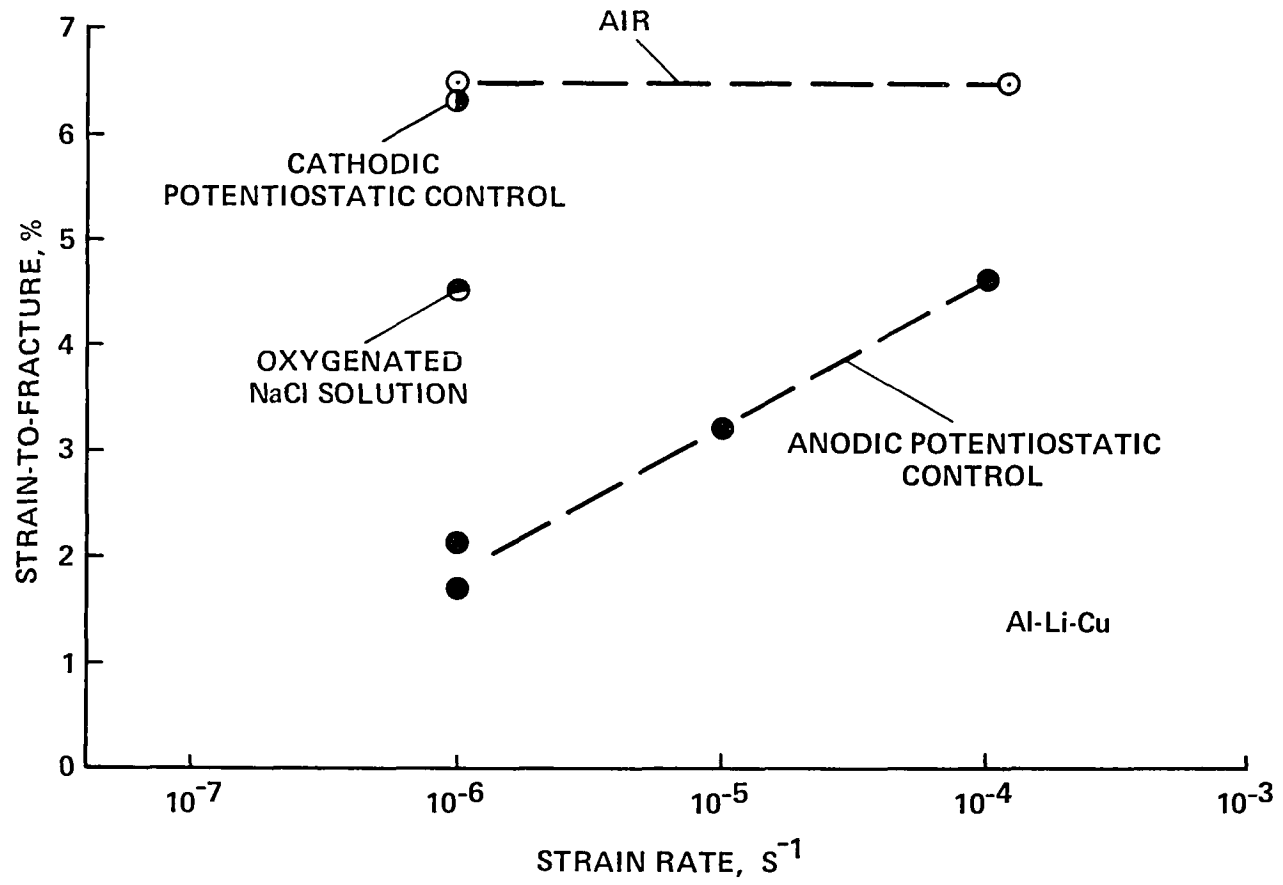


Figure 10.- The stress corrosion susceptibility at various applied potentials; slow strain-rate test data.

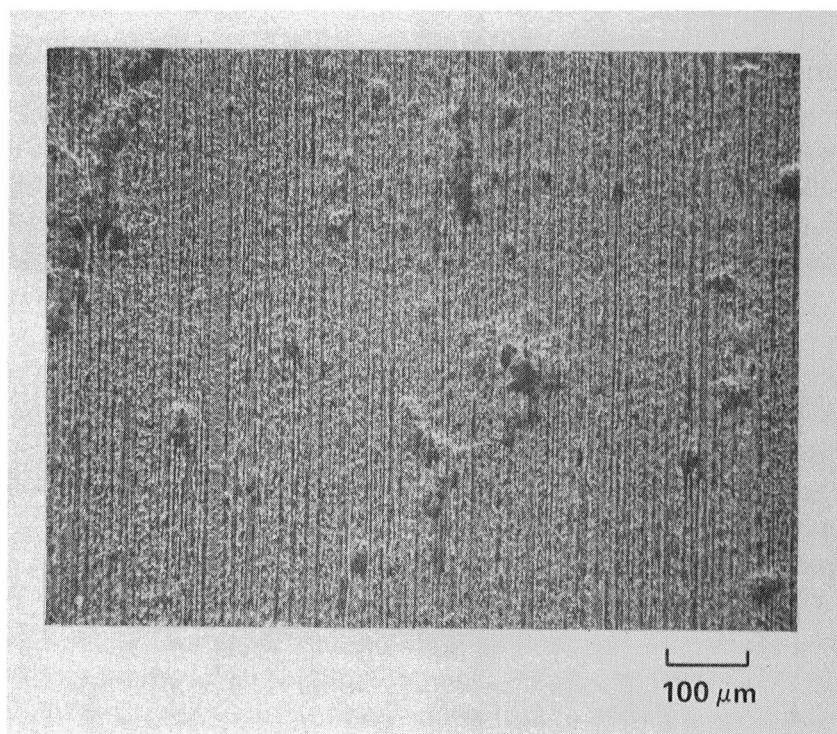


Figure 11, - Surface pits on Al-Li-Cu alloy, straining electrode specimen exposed to a deaerated aqueous 3,5% NaCl solution under cathodic potentiostatic control. ($-1.075 V_{sce}$),

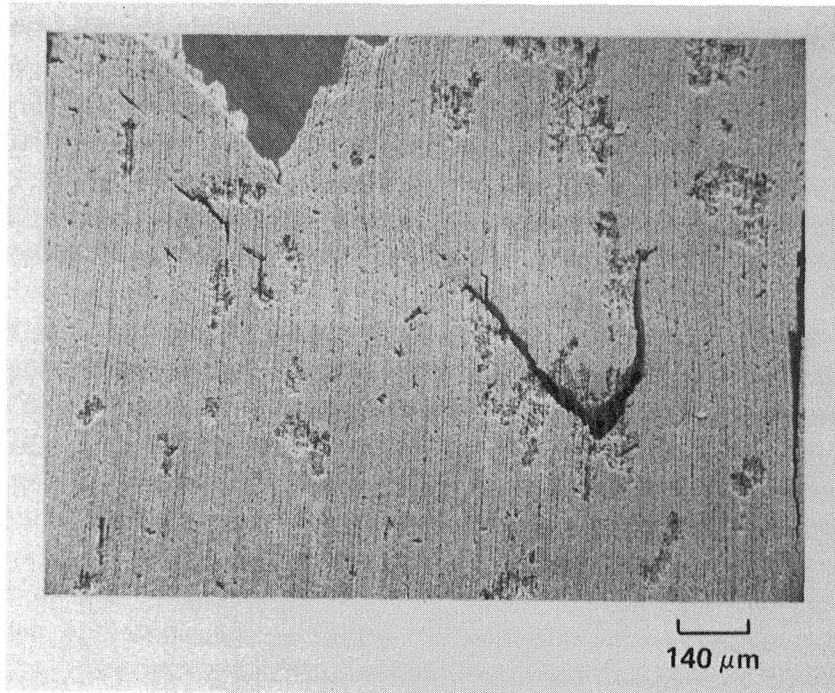
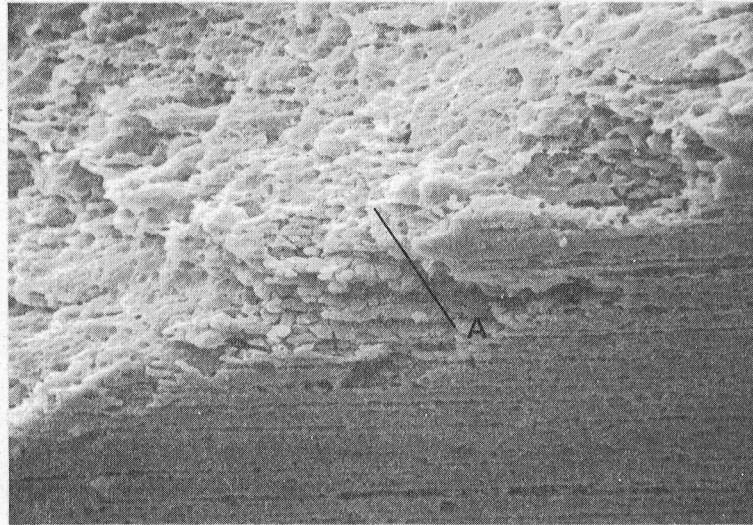
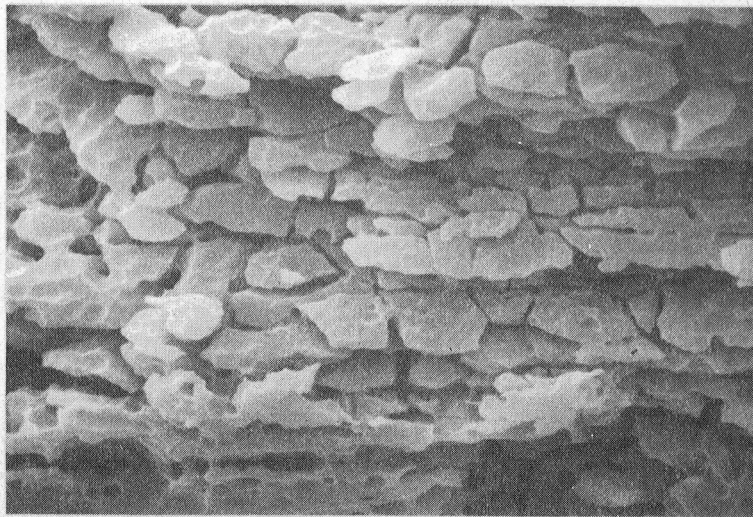


Figure 12.- Surface of Al-Li-Cu alloy, straining electrode specimen exposed to deaerated, aqueous 3.5% NaCl solution under anodic potentiostatic control ($-0.850 V_{sce}$). Note secondary cracks near primary fracture associated with the large surface pits.



a)

20 μm



b)

.05 μm

Figure 13.- Intergranular pitting associated with final fracture of Al-Li-Cu alloy, straining electrode specimen at unmasked surface (10^{-6} s^{-1} , $-0,850 \text{ V}_{\text{sc}}^{\text{e}}$):
(a) Surface/fracture interface, (b) Surface topography within pit, A.

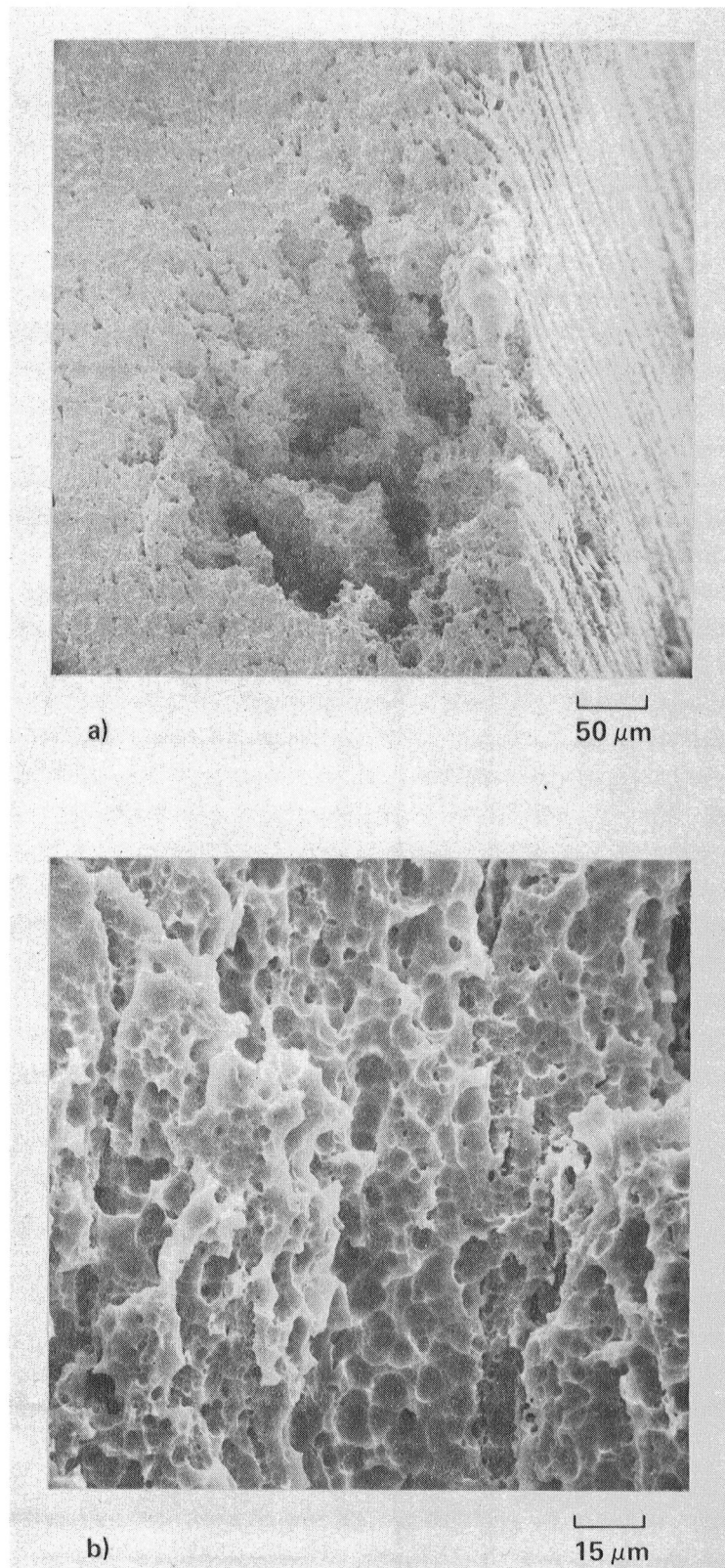


Figure 14.- Fracture surface of Al-Li-Cu alloy, straining electrode specimen tested under free-corrosion conditions in an oxygenated, aqueous 3.5% NaCl solution: (a) Primary fracture showing large pit near specimen surface. (b) Surface topography within the large pit.

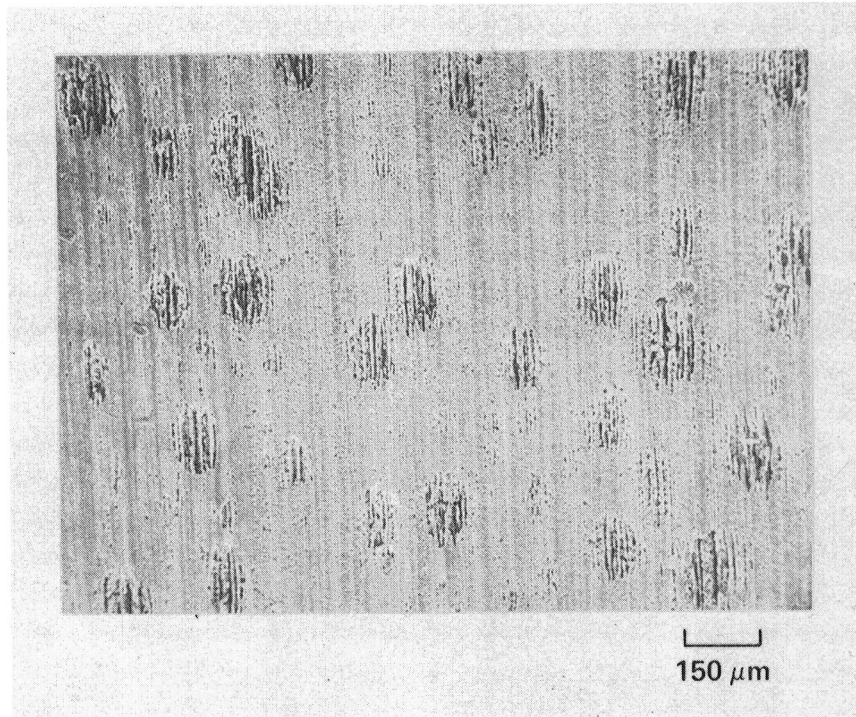
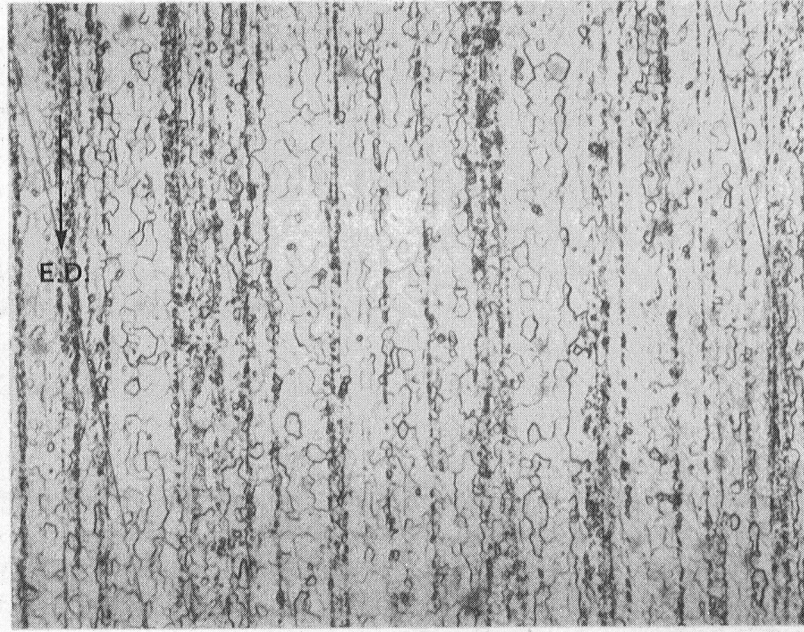
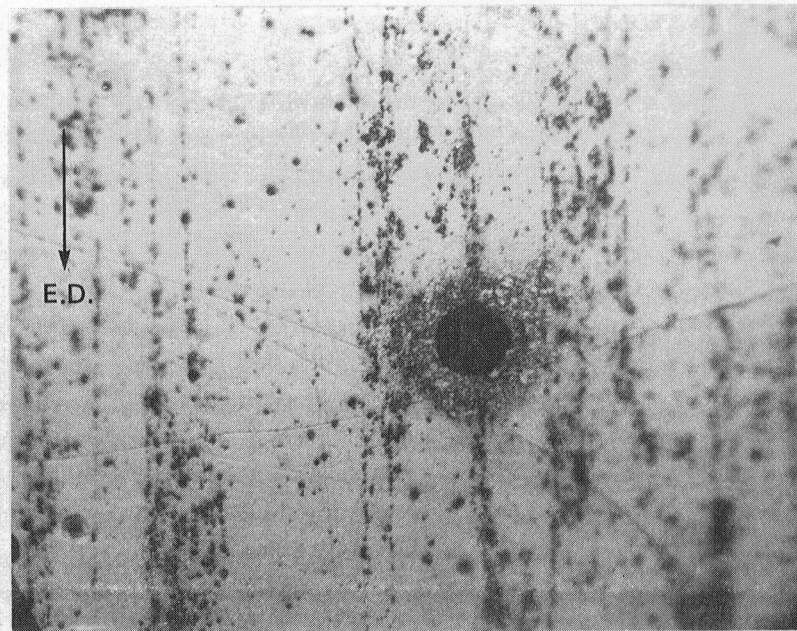


Figure 15.- Surface pits on Al-Li-Cu alloy, straining electrode specimen exposed to an oxygenated, aqueous 3.5% NaCl solution under free-corrosion conditions.



a)

50 μm



b)

25 μm

Figure 16.- A comparison between microstructure and pitting in the Al-Li-Cu alloy; E.D. signifies the extrusion direction. (a) Underlying microstructure. (b) Surface pitting following 16-h exposure to deaerated, aqueous 3.5% NaCl solution under anodic potentiostatic control ($-0.850 V_{s_{ce}}$).

1. Report No. NASA TM-84287	2. Government Accession No.	3. Recipient's Catalog No.	
4. Title and Subtitle THE STRESS-CORROSION BEHAVIOR OF Al-Li-Cu ALLOYS: A COMPARISON OF TEST METHODS		5. Report Date September 1982	
		6. Performing Organization Code	
7. Author(s) Patrick P. Pizzo,* Ray P. Galvin, and Howard G. Nelson		8. Performing Organization Report No. A-9057	
		10. Work Unit No. T-9516B	
9. Performing Organization Name and Address NASA Ames Research Center Moffett Field, Calif. 94035		11. Contract or Grant No.	
		13. Type of Report and Period Covered Technical Memorandum	
12. Sponsoring Agency Name and Address National Aeronautics and Space Administration Washington, D.C. 20546		14. Sponsoring Agency Code 505-33-21	
		15. Supplementary Notes *San Jose State University, San Jose, Calif. 95192. Point of Contact: Howard G. Nelson, Ames Research Center, MS 230-4, Moffett Field, Calif. 94035. (415) 965-6137 or FTS 448-6137.	
16. Abstract <p>The stress-corrosion (SC) behavior of two powder metallurgy processed (Al-Li-Cu) alloys with and without Mg addition in aqueous 3.5% NaCl solution has been investigated. Three test techniques were employed in the investigation: the alternate-immersion testing of tuning fork specimens, slow crack-growth tests using fracture-mechanics specimens, and the slow strain-rate testing of straining electrode specimens. The corrosion conditions investigated include cathodic and anodic potentiostatic control and free-corrosion under constant-immersion and alternate-immersion conditions. The heat treatment and the orientation of the alloys were varied to establish the more susceptible material conditions. Scanning electron microscopy and optical metallography were used to demonstrate the character of the interaction between the Al-Li-Cu alloys and the selected environment.</p> <p>Both Al-Li-Cu alloys are susceptible to SC in an aqueous 3.5% NaCl solution under the right electrochemical and microstructural conditions. Each test method was found to yield important information on the character of the SC behavior. Under all conditions investigated, second-phase particles strung out in rows along the extrusion direction in the alloys were rapidly attacked, and they play a principal role in the SC process. With time, larger pits develop from these rows of smaller pits and under certain electrochemical conditions surface cracks initiate from the larger pits and contribute directly to the fracture process. Evidence to support slow crack growth was observed in both the slow strain-rate tests and the sustained-immersion tests of precracked fracture-mechanics specimens. The possible role of H₂ in the stress-corrosion cracking process is suggested.</p>			
17. Key Words (Suggested by Author(s)) Aluminum-lithium-copper Stress corrosion Potentiostatic polarization		18. Distribution Statement Unlimited Subject Category: 26	
19. Security Classif. (of this report) Unclassified	20. Security Classif. (of this page) Unclassified	21. No. of Pages 46	22. Price* A03

